electrochem

MDPI

Article

Tape Casting of NASICON-Based Separators with High Conductivity for Na All-Solid-State Batteries

Melanie Rosen [1], Samir Mahioui [2], Christian Schwab [1], Gerald Dück [1] and Martin Finsterbusch [1,3,*]

[1] Forschungszentrum Jülich GmbH, Institute of Energy Materials and Devices, Materials Synthesis and Processing (IMD-2), 52425 Jülich, Germany
[2] TU Darmstadt, Institute of Materials Science, Otto-Berndt-Str. 3, 64287 Darmstadt, Germany
[3] Forschungszentrum Jülich GmbH, Helmholtz-Institute Münster: Institute of Energy Materials and Devices, (IMD-4), 52425 Jülich, Germany
* Correspondence: m.finsterbusch@fz-juelich.de

Abstract: Sodium–ion batteries are emerging as strong competition to lithium–ion batteries in certain market sections. While these cells do not use critical raw materials, they still feature a liquid electrolyte with all its inherent safety issues, like high flammability and toxicity. Alternative concepts like oxide-ceramic-based all-solid-state batteries feature the highest possible safety while still maintaining competitive electrochemical performance. However, production technologies are still in their infancy, especially for Na all-solid-state batteries, and need to be urgently developed to enable solid-state-battery technology using only abundant raw materials. In this study, the additive-free production of freestanding, undoped NaSICON separators via tape-casting is demonstrated, having an extremely high total Na-ion conductivity of up to 2.44 mS·cm^{-1} at room temperature. Nevertheless, a strong influence of sample thickness on phase purity as well as electrochemical performance is uncovered. Additionally, the effect of self-coating of NaSICON during high-temperature treatment was evaluated as a function of thickness. While advantageous for increasing the stability against Na-metal anodes, detrimental consequences are identified when separator thickness is reduced to industrially relevant values and mitigation measures are postulated.

Keywords: solid-state-batteries; NaSICON; tape-casting

Academic Editor: Cataldo Simari

Received: 20 December 2024
Revised: 23 January 2025
Accepted: 8 February 2025
Published: 16 February 2025

Citation: Rosen, M.; Mahioui, S.; Schwab, C.; Dück, G.; Finsterbusch, M. Tape Casting of NASICON-Based Separators with High Conductivity for Na All-Solid-State Batteries. *Electrochem* **2025**, *6*, 5. https://doi.org/10.3390/electrochem6010005

1. Introduction

The targeted switch to renewable energies all over the world inevitably leads to the question of energy storage, with batteries as one of the most efficient options for short- and medium-term storage. Thus, demand for batteries is rising, and with expected growth rates, the supply risk for some critical raw materials is becoming a concern. Therefore, the European Union has addressed this issue with a plan for the use of critical materials, including lithium and cobalt [1], and researchers worldwide are looking to close this gap with alternative battery chemistries that do not rely on these materials.

Sodium-based cells have been established as a valid competitor to LIBs, with the first commercial sodium–ion cells already available on the market in China (CATL, Ningde, China; HiNa Battery Technology, Liyang, China). These cells successfully avoid critical raw materials, but they still feature a liquid electrolyte with all its inherent safety issues, like high flammability and toxicity. While alternative concepts like the ZEBRA battery use a non-flammable ceramic separator made from β″-Alumina [2], it operates at around 300 °C and has a molten sodium anode [3], which limits its applicability and comes with additional safety concerns.

To reach maximum safety and widen application possibilities, true all-solid-state Na batteries (Na-ASBs) with Na-metal anodes and high capacity (mixed-phase) cathodes that can be operated at room temperature need to be developed. Such a Na-ASB could fill the above-mentioned gap and provide a battery technology only using abundant raw materials, featuring the highest possible safety and still maintaining competitive electrochemical performance.

In such a Na-ASB, the most crucial component is the solid-ceramic electrolyte since it connects all parts of the cell. In this regard, the large family of materials with a Natrium Super Ion Conductor (NaSICON) crystal structure, like $Na_{1+x}Zr_2Si_xP_{3-x}O_{12}$ [4], shows excellent ionic conductivity at room temperature and high stability with metallic sodium. While a wide variety of substitutions has been examined [5,6], Scandium has shown the highest ionic conductivity [7]. Fortunately, extremely high conductivities of ~5 mS·cm^{-1} can already be reached for the pure material by tightly controlling the sodium content [8,9]. Additionally, the as-synthesized surface of these materials already displays high compatibility with sodium metal [10], allowing for dendrite-free cycling up to 14 mAh cm^{-2}, facilitated by the formation of Na_3PO_4 nanolayers originating from the high volatility of Na and P during the high-temperature sintering of NaSICON-pellets [11]. While the volatility of these elements has previously been discussed in the context of phase purity and the formation of ZrO_2 secondary phase [12–15], the formation of Na_3PO_4 has only been mentioned briefly.

For the manufacturing of ceramic components, tape casting is a well-established, easily scalable method for producing large, flat layers needed for stacking multi-cell batteries. Surprisingly, in stark contrast to lithium batteries, only a very few publications have explored the tape casting of NaSICON-based materials, and tape casting of separators for Na batteries is reported even more scarcely.

The screen-printing of NaSICON materials for CO_2-sensor production was first reported in 1984 [16] and has since become an established process [17–20], where conductivities in the 0.5 mS·cm^{-1} range are reported. However, it relies on ceramic substrates as structural support and is therefore not suitable for battery production. In ZEBRA-type batteries, beta-alumina separators have been scaled to 100 mm diameter, but total Na-ion conductivities of only 0.2 mS·cm^{-1} at 300 °C are reported [21]. Finally, for NaSICON-type materials, the successful production of thin separators has thus far mostly relied on sintering aids [22,23], with reported conductivities of 0.2–0.4 mS·cm^{-1}, or the introduction of dopants like Y [24,25], with reported conductivities above 1 mS·cm^{-1} for $Na_5YSi_4O_{12}$, which still falls short of the high conductivities possible within this class of material.

To improve compatibility with the Na-metal anode, recent work by Jaschin et al. [26] reported the fabrication of dense-porous multilayers via tape casting of Zn-Mg-co-doped NaSICON. By introducing a coating with ZnO to the porous scaffold, critical current densities of 40 mA cm^{-2} were reached in symmetrical cells. However, the conductivity of the dense layer separators was not reported. In an alternative approach, the excess of Na and P in thick NaSICON pellets was shown to counteract evaporation losses during high-temperature sintering, leading to the in situ formation of a Na_3PO_4 surface coating on the pellets [11]. This also significantly reduced the interface resistance with metallic sodium.

In this work, we report for the first time the tape casting of undoped NaSICON separators and their processing into thin, free-standing separators with total Na-ion conductivities > 2 mS·cm^{-1} at room temperature. Additionally, we investigate the in situ formation of surface coatings and their effect on the electrochemical performance of the produced separators, underlining the critical need to understand and effectively control the loss of volatile species to enable the production of high-quality NaSICON separators with minimized thickness.

2. Experimental Methods

2.1. Powder Synthesis, Reference Pellets, and Powder Optimization

The NaSICON powder with the $Na_3Zr_2Si_{2.3}P_{0.7}O_{11.85}$ composition was synthesized via a solution-assisted solid-state reaction as reported previously [27]. $NaNO_3$ (Merck, ACS grade), $ZrO(NO_3)_2 \cdot x\ H_2O$ (Aldrich, 99%), $Si(OCH_2CH_3)_4$ (Merck, 99%), $NH_4H_2PO_4$ (Merck, 99%), and HNO_3 (69%, Aldrich, ACS grade, Washington, DC, USA) were used as reactants. The solution was stirred overnight on a hotplate at 80 °C, allowing a significant portion of the aqueous solution to evaporate, leaving behind a white gel. This gel was transferred to a drying oven and further dried at 80 °C for about 5 days, resulting in the formation of a white powder. The resulting powder was milled in an electric mortar for 1 h and calcined in air at 760 °C for 10 h.

To prepare sintered reference pellets, the calcined powder was uniaxially pressed into pellets with a 13 mm diameter at 75 MPa and sintered in a closed crucible at 1260 °C for 7 h, with heating and cooling rates of 2 K min^{-1}.

To adjust the particle size distribution for the tape-casting process, the NaSICON powder was wet-milled in ethanol in a planetary ball mill (PM400, Retsch, Haan, Germany) in a 125 mL ZrO_2 jar with 3 mm ZrO_2 milling balls at 600 rpm for 120 min. The ratio of powder to milling balls was fixed at 1:13.75 by weight.

2.2. Slurry Fabrication and Tape Casting

A schematic representation of the sample preparation route is displayed in Figure 1.

Figure 1. Schematic representation of the sample preparation route.

A solution of the binder (PVB98, Sigma Aldrich, Burlington, MA, USA), additives (PEG400, Sigma-Aldrich and Solusolv, Solutia Inc., Springfield, MA, USA), and dispersant (BYK 180, Altana, Wesel, Germany) in a mixture of butanone (VWR, 99.6%) and ethanol (VWR, 99.6%) was homogenized in a planetary mixer (Thinky, Tokyo, Japan) at 1500 rpm for two minutes and set on a roller bench for 24 h to homogenize. Subsequently, the ceramic powders were added and homogenized again in the planetary mixer. The obtained slurry was cast onto a Mylar foil with a fixed gap height of 500 µm. After drying at room temperature for 10 h, the obtained green tapes were laminated under 150 MPa at 50 °C for 2 min. After pressing, the green tapes were cut into 12 mm diameter discs and transferred into an Al_2O_3 crucible. The tapes were sintered into NaSICON pellets at 1260 °C in air for 7 h, with heating and cooling rates of 4 K min^{-1}, to obtain free-standing separators. The pellets were sintered at 1260 °C for 7 h in air and passivated through an additional temperature treatment at 1260 °C for 20 h in air.

2.3. Characterization

The particle size distribution of the powders was checked carefully via laser diffraction using an LA950 (Horiba Scientific, Irvine, CA, USA) with 650 nm and 405 nm laser sources. The data were analysed using the Mie model.

The phase purity was assessed through X-ray diffraction measurements (Bruker D4 Endeavor with a 1D LYNXEY detector and monochromatized Cu-Kα radiation). Grazing incident measurements at an incident angle of 0.1° were performed on an Empyrean (Malvern PANalytical, Malvern, UK). Symmetric theta/theta scans were performed ap-

plying the focusing Bragg–Brentano geometry, with a parallel X-ray beam mirror attached to the primary optic side with a fixed divergence slit of 0.25°, and a 0.18° parallel plate collimator was used as a secondary optic in front of the proportional detector. The scans were carried out using Cu-Kα radiation (45 kV, 40 mA), covering Bragg angles between 25° and 85°, with a step size of 0.05° and a scanning duration of 3 s per step.

A cross-section was prepared by embedding the sintered tapes in epoxy resin (EpoFix Resin Harz and EpoFix Hardener). The embedded samples were polished with 4000-grit SiC sandpaper and finished with a 1 µm diamond suspension. The polished cross-sections and the morphology of the primary powder particles were analysed using a scanning electron microscope (TM3000, Hitachi, Tokyo, Japan).

A Renishaw InVia Raman Microscope equipped with a solid-state excitation laser (532 nm) and a 2400 lines/mm grating was used to collect Raman spectra. The exposure time per spectrum was set to 1 s. The Wire 5.2 software (Renishaw, Dundee, IL, USA) was applied to remove the cosmic rays from the raw data. Normalization of the spectra to the maximum height between 600 cm^{-1} and 700 cm^{-1} and subsequent averaging was performed using an in-house developed Python script.

To determine the surface depletion of Na in NZSP tapes, Time-of-Flight Secondary Ion Mass Spectrometry (TOF-SIMS) depth profiles were recorded. Measurements were performed on a TOF-SIMS.5 NCS system (IONTOF GmbH, Germany) equipped with a Bi-Nanoprobe 50 primary ion gun, an oxygen sputter gun, and a low-energy electron flood gun for charge compensation. Additional charge compensation was accomplished by Ar main flooding at a pressure of 2×10^{-6} mbar. Bi+ primary ions were used for analysis at an energy of 30 keV and 1 keV oxygen ions for sputtering. Depth profiles were recorded in positive polarity with an analysis raster of 50 µm × 50 µm at 128 × 128 pixels in spectrometry mode, while the oxygen sputter raster was set to 250 µm × 250 µm.

Gold blocking electrodes were sputtered onto the freshly sintered pellets surfaces (2 min sputter time, Cressington 108auto Coater, Watford, UK). The pellets were placed in Swagelok cells for impedance measurement at 25 °C. The voltage amplitude was set to 20 mV, and the frequency varied from 7 MHz to 1 Hz (VMP-300 multipotentiostat, BioLogic, Orlando, FL, USA). The formula, $\sigma = d/(R \cdot A)$, was used to calculate the conductivity, with the resistance R, the sample thickness d, and the geometric surface area A.

Impedance measurements at elevated and reduced temperatures were performed (Novocontrol Technologies Alpha-A) in a frequency range from 10 MHz to 1 Hz, applying a voltage amplitude of 20 mV. The temperature was varied between −100 °C and 100 °C in a temperature-controlled chamber (Novocontrol Technologies BDS1100, Forest, NC, USA).

Data analysis and equivalent circuit simulation were performed within the Relaxis3 software V3.0.23.25. The Nyquist plots were normalized to the sample geometry. An Arrhenius plot according to the Arrhenius equation: $\sigma T \sim \exp[-E_a/(kT)]$, with the ionic conductivity σ, the Boltzmann constant k, and the absolute temperature T, was linearly fit to determine the activation energy E_a.

3. Results

3.1. Powder Preparation for Tape Casting

While solution-assisted solid-state synthesis is a well-established process for the production of high-conductivity NaSICON materials, the control and reproducibility of the particle size distribution after synthesis is challenging in lab-scale production (Figure 2a). Therefore, a wet-milling process was introduced into the production chain to ensure precise control over the PSD and the resulting rheological properties of the slurry in the subsequent tape-casting process. After milling and drying, the mean particle size was determined to be 4.5 µm, with a monomodal particle size distribution (Figure 2b). The cuboidal shape

of the particles remained mostly intact during milling, which was confirmed via SEM (Figure 2c,d). The SEM images of the milled powder also show isolated grains with a brighter material contrast (Figure 2c,d), corresponding to the existence of ZrO_2. XRD measurement of the powder showed a high phase purity for NaSICON (ICSD No. 202154), with a small amount of secondary ZrO_2 phase (Figure 3a, secondary phase marked with *, ICSD 60900). The presence of ZrO_2 has already been reported in literature as a typical secondary phase in NaSICON materials [12–15], but low contents have been shown to have no detrimental effects on the electrochemical properties.

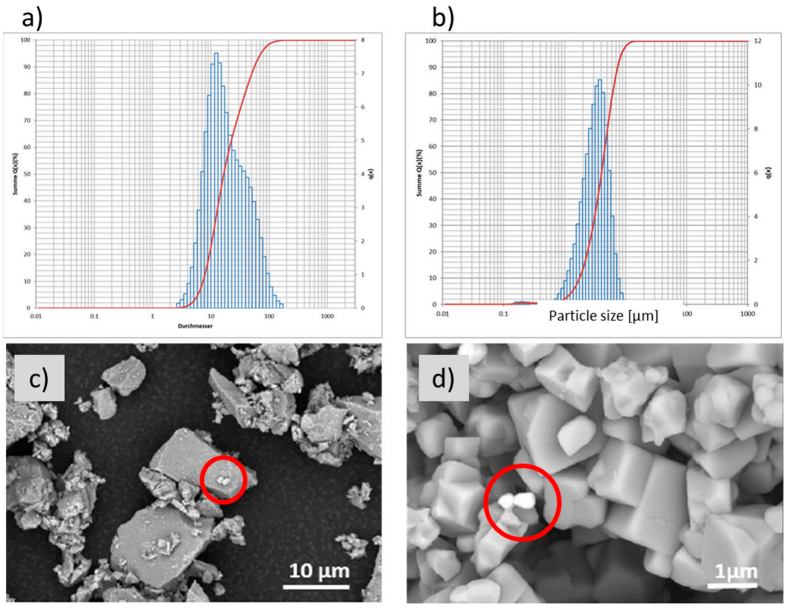

Figure 2. Particle size distribution and SEM images of NZSP powder: (**a**) before and (**c**) after synthesis, (**b**) before and (**d**) after milling. Small impurities of ZrO_2 are visible as brighter particles (red circles).

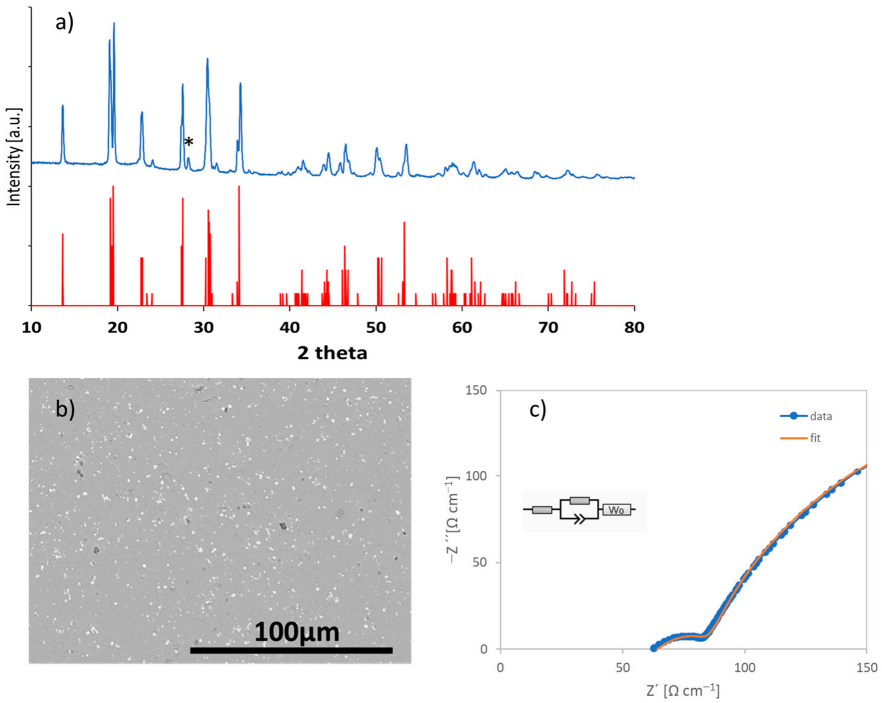

Figure 3. (**a**) XRD of as-synthesized NaSICON powder, with secondary ZrO2 phase marked by *; (**b**) SEM cross-section of a sintered pellet; (**c**) room temperature impedance of the powder-pressed sample sintered at 1260 °C.

3.2. Basic Characterization of Benchmark Pellets

To establish a baseline for ionic conductivity, a sample from this material was uniaxially pressed and sintered at 1260 °C for 6 h. The resulting pellets had a thickness of 12.5 mm, and their relative density, determined using Archimedes' method, was 98.15%. The pellets still showed small inclusions of secondary ZrO_2 phase (Figure 3b). Equivalent circuit simulation of the impedance data (Supplementary Table S1) revealed that the distinguishable semi-circle corresponds to the grain boundary (GB) resistance, with a capacitance of 1.75×10^{-9} F. The bulk resistance could not be distinguished at room temperature. The total ionic conductivity was therefore determined to be 2.18 mS·cm^{-1} (Figure 3c). These values will be used as the baseline for evaluating the effect of the tape-casting process on the component properties.

3.3. Tape Casting of Thin Separators

The tape-casting process was adapted from our previous work [28], with only slight modifications to the amount of dispersant (adjusted to the different surface termination of the NaSICON material) and the solvent content (optimized for the established particle size distribution). The fixed height of the gap-bar coater allowed for high reproducibility of the green body thickness at 100 µm, while higher sample thicknesses can be realised by laminating several green tape layers during the compaction step. In this study, the green body thickness was varied between 100 µm and 400 µm. During the subsequent high-temperature sintering step, sufficient sample flatness must be ensured to facilitate electrochemical testing. Additionally, the substrate should not introduce changes to the contacting particle surface through interdiffusion of elements. Therefore, the green tapes were placed on sintered and passivated NaSICON pellets ("mother pellets") during high-temperature treatment. Flat separators with relative densities above 92% were produced (Figure 4a).

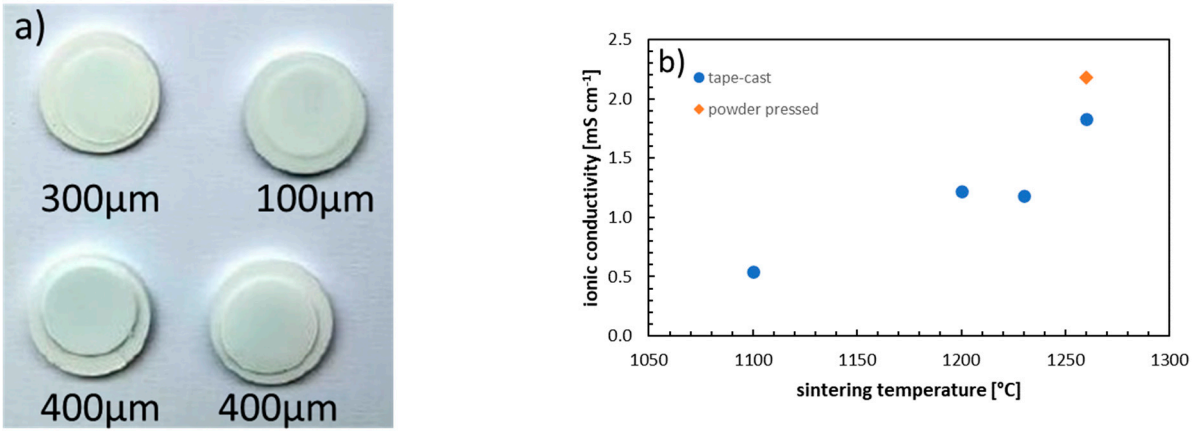

Figure 4. (**a**) Photograph of the tape-cast separators after sintering on the mother pellets; (**b**) total Na-ion conductivity at room temperature of the tape-casted separators sintered at different temperatures.

To evaluate the influence of the drastically reduced sample thickness compared to powder-pressed samples, the sintering temperature was varied between 1100 °C and 1260 °C for separators with a medium thickness of 250 µm. While suitable ionic conductivities > 1 mS·cm^{-1} were already achieved at 1200 °C and 1230 °C, a significant improvement to 1.83 mS·cm^{-1} was achieved by sintering the separators at 1260 °C (Figure 4b).

XRD measurements (Figure 5a) confirm the unchanged phase purity when comparing the tape-cast samples to the baseline powder-pressed pellets. The tape-cast samples also show ZrO_2 as a secondary phase. The small grains (Figure 5b), which were already detected in the powder via SEM, are still present in the cross-section of the sintered tape, with no

detectable changes in particle form or size. As they do not significantly obstruct the pathways for sodium conduction, no detrimental effects on the electrochemical properties are expected.

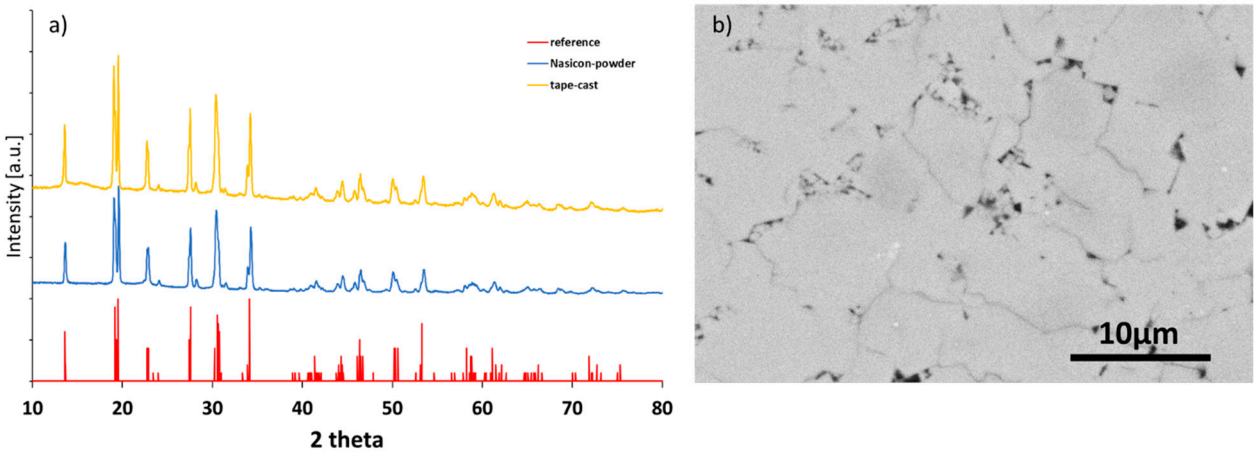

Figure 5. (**a**) XRD pattern of the tape-cast NaSICON separators; (**b**) polished cross-section of the sintered NaSICON tape.

3.4. Effect of Volatile Species During Sintering

To elucidate the effect of volatile species and possible surface film effects, like the known formation of Na_3PO_4 nanolayers, the influence of sample thickness on the separator properties was investigated. By laminating different numbers of green tapes, different stacking heights were achieved, thus effectively adjusting the surface area-to-bulk volume ratio. After sintering at 1260 °C, the resulting separators had thicknesses of 98 µm, 293 µm, and 393 µm. XRD measurements of all samples were performed to investigate the influence of sample thickness on phase purity. For the highest investigated sample thicknesses, the phase purity matched that of the baseline powder-pressed samples (Figure 6a). In contrast to these findings, thinner samples of 100 µm and 300 µm displayed a higher content of ZrO_2. The formation of these secondary phases has been reported in literature [29] to be related to the loss of phosphorous-containing species during high-temperature treatment. This effect is present in all investigated tape-cast samples, but its influence on the properties of the samples increases as the ratio of sample surface area to bulk sample volume increases drastically when lowering the sample thickness.

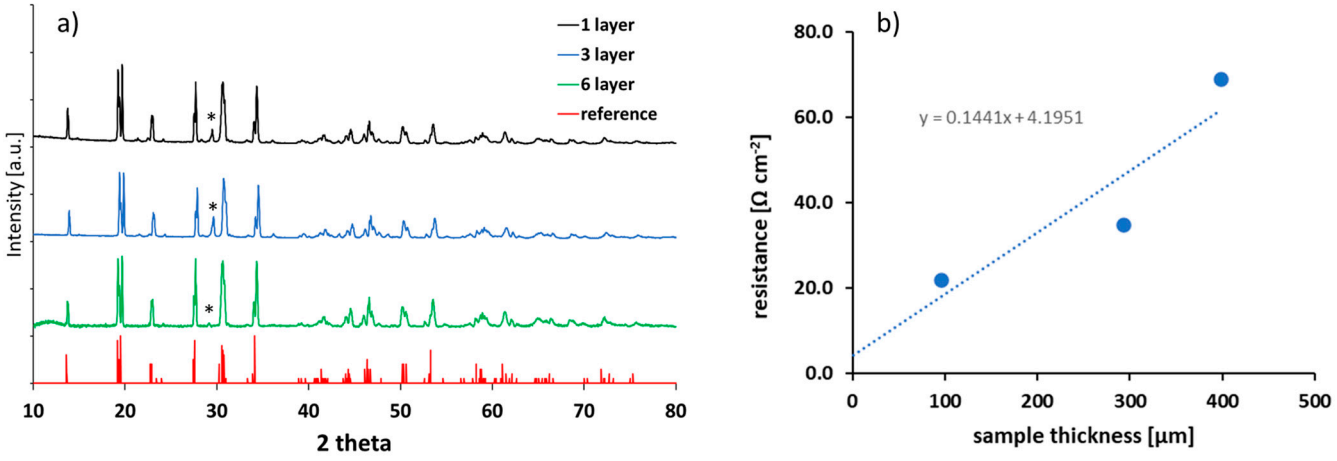

Figure 6. (**a**) XRD patterns of tape-cast samples with various thicknesses, * indicates a secondary ZrO_2 phase; (**b**) area-normalized resistance of separators with various thicknesses.

Using this approach, a relation between sample thickness and the absolute ionic conductivity of the separator was uncovered.

The 400 µm-thick sample showed an outstanding total Na-ion conductivity of 2.44 mS·cm^{-1} at room temperature, even outperforming the powder-pressed samples. In contrast, the thinner samples fell significantly short. The 300 µm thick sample displayed a reduced room-temperature ionic conductivity of only 1.83 mS·cm^{-1}, while the 100 µm sample displayed an even more pronounced reduction to 1.75 mS·cm^{-1} at room temperature, even though the content of secondary phases is very similar for separators with thicknesses between the 300 µm and 100 µm. As this proportional connection of sample thickness and reduced ionic conductivity indicates a detrimental surface modification below the detection limits of XRD analysis, additional analysis with higher surface sensitivity is needed.

3.5. Surface Layer Investigation

Raman analysis of the sintered samples (Figure 7a) shows NaSICON and ZrO_2, as well as the presence of $Na_2ZrSi_2O_7$ as an additional secondary phase, which can also be attributed to the loss of volatile P during high-temperature treatment. To determine whether the detrimental surface coating consists of $Na_2ZrSi_2O_7$, Raman measurements were repeated after dry-polishing the sample with 4000 grit sandpaper to remove the surface layer (Supplementary Figure S1). The spectrum of the polished sample shows an increase in peak height for $Na_2ZrSi_2O_7$, proving the existence of this secondary phase also in deeper layers of the sample. It can be assumed that this phase is present throughout the sample and, therefore, is not responsible for the thickness-related conductivity loss.

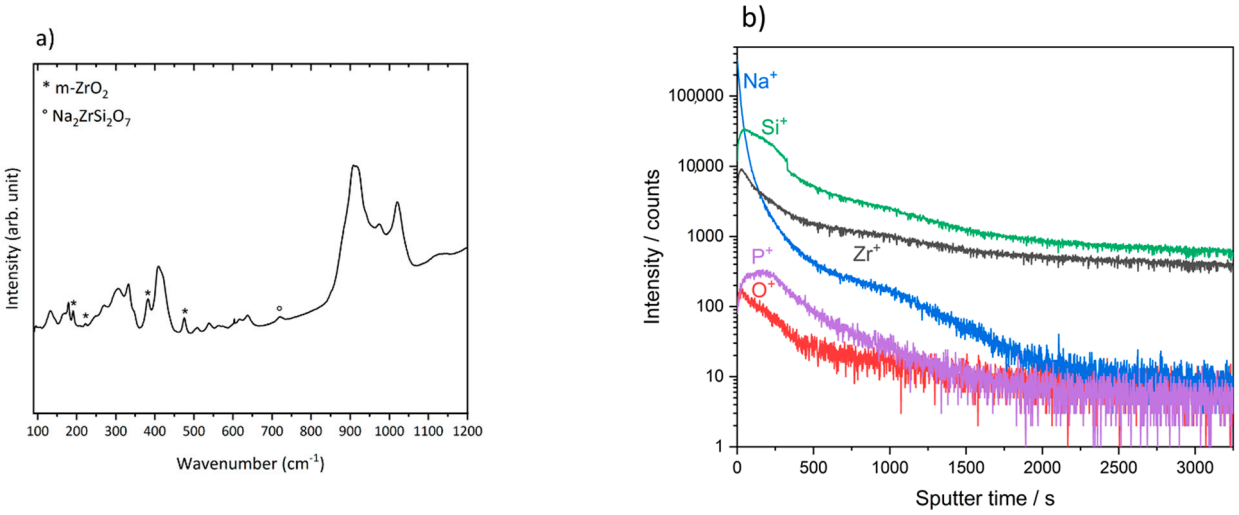

Figure 7. (**a**) Raman analysis of the sample surface; (**b**) SIMS analysis of the sample surface.

SIMS analysis of the as-sintered sample surface was performed to uncover the chemical composition of the surface layer (Figure 7b). While the Zr^+, Si^+, and O^+ signals display similar intensity decreases with increasing sputter time, the P^+ signal exhibits a surface-near plateau before decreasing similarly to the other elements. In strong contrast, the Na^+ signal significantly decreases during the surface-near P^+ plateau before following the trend of the other elements. These findings further indicate the formation of a surface layer containing elevated concentrations of Na and P compared to the NaSICON material itself. Since the intensities in SIMS measurements strongly depend on the embedding matrix of the elements and are not quantitative, no conclusions about the exact composition of the surface coating can be drawn. Additionally, due to the uneven surface of the sample, AFM measurements to correlate the data with corresponding depths were not possible.

Nevertheless, the distinct P^+ plateau and the matching change in slope of the Na^+ signal indicate a surface coating with a well-defined thickness and boundary.

SIMS analysis of the as-sintered sample surface was performed to uncover the chemical composition of the surface layer (Figure 7b). The analysis reveals four distinct layers. In the topmost layer, the Na^+ concentration decreases, while the signals of the remaining species increase. This is followed by a plateau in the P^+ signal and a further decrease in Na^+, indicating the presence of a Na- and P-rich surface coating.

To uncover the nature of this surface coating, grazing incident XRD measurements were performed to increase surface sensitivity (Figure 8). At an incident angle of 0.1°, an additional, broadened peak can be distinguished at 21.3° (2Θ), identifying the surface coating as Na_3PO_4. While the self-coating properties of NaSICON during high-temperature treatment have been reported for pellets with thicknesses around 1.5 mm, the coating's effect was only viewed in light of its positive effects on the wetting of sodium [11]. Unfortunately, due to this high thickness, its detrimental effects on reduced conductivity have not been observed so far.

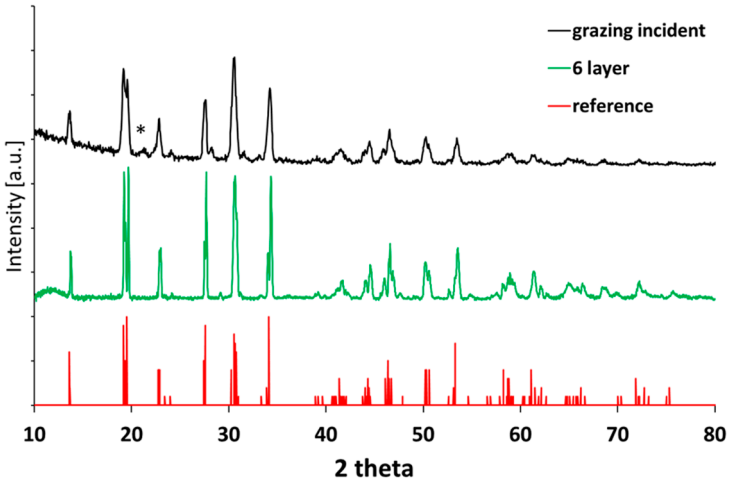

Figure 8. Grazing incident XRD of sintered separators, with the Na_3PO_4 phase marked by *.

To gain a more detailed insight into the electrochemical properties, temperature-dependent electrochemical impedance spectroscopy measurements were performed on samples with a thickness of 400 µm. At room temperature, within the observed frequency range, no distinction between bulk and grain boundary resistance could be made (Figure 9a). Here, only the very high total Na-ion conductivity of 2.44 $mS \cdot cm^{-1}$ is reported. However, at a reduced temperature of −100 °C, two clearly distinguishable semicircles can be observed (Figure 9b). The semicircle at high frequencies corresponds to the bulk resistance, with a capacity of $0.66 \cdot 10^{-12}$ F, resulting in a bulk conductivity of 3.55 $mS \cdot cm^{-1}$. The semicircle at medium frequencies corresponds to the grain boundary resistance, with a capacity of $0.25 \cdot 10^{-9}$ F. The low-frequency tail, represented by the Warburg element, stems from the use of blocking electrodes. The activation energies, derived from the Arrhenius plot of the temperature-dependent impedance spectroscopy data (Figure 9c), reveal a total activation energy of 0.27 eV, which matches the literature values for this composition of NaSICON exactly [8].

Unfortunately, the resistance contribution from the thin Na_3PO_4 surface coating is still not visible at −100 °C within the available frequency range. In order to obtain at least some information on the electrochemical properties of the Na_3PO_4 surface coating, a linear fit of the area-normalized resistance of the sintered separators with varying thickness was performed (Figure 6b). The intersection of the linear fit with the y-axis is at around 4 Ω, which is much smaller than the 20 to 60 Ω total resistance of the samples. While

this is the obvious reason that the detrimental effect on conductivity was hidden in the thick pellet-type samples, it clearly shows that the low conductivity of the Na_3PO_4 surface coating cannot be neglected in industrial-type samples. Here, thicknesses around 10–20 µm are targeted, which means that the total resistance induced by the surface layer could be the same or even higher than the total resistance of the (bulk) NASICON separator. Clearly, ways to modify the surface of thin NASICON separators need to be investigated to achieve high stability against Na metal while having low impedance.

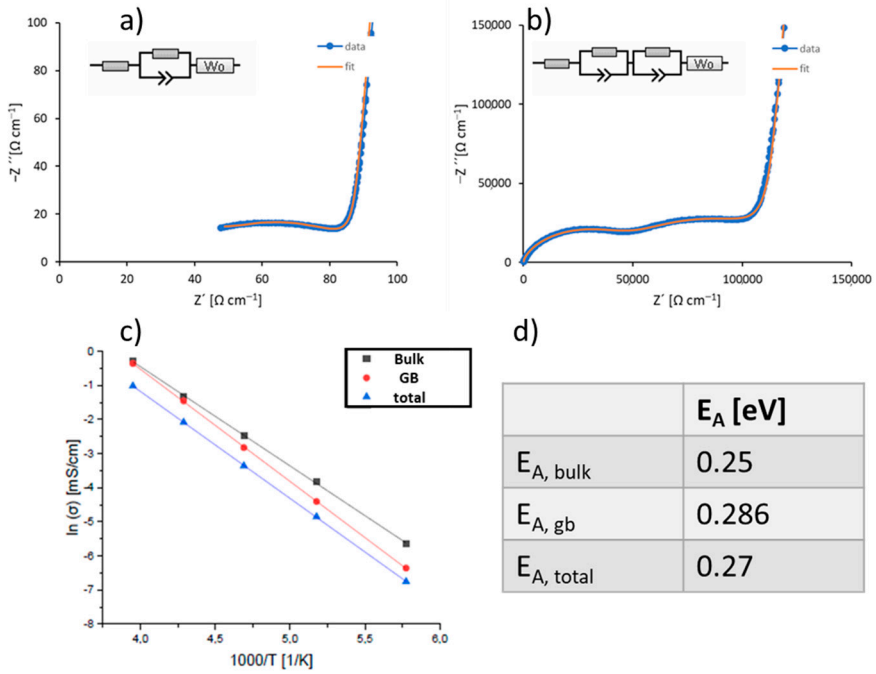

Figure 9. (**a**) Impedance measurement of sintered tape-cast sample at 25 °C; (**b**) impedance measurement of sintered tape-cast sample at −100 °C; (**c**) Arrhenius plot of the ionic conductivity of tape-cast NaSICON; (**d**) table of activation energies derived from the Arrhenius plot.

Nevertheless, even our thinnest reported samples, with a total Na-ion conductivity of 1.75 mS·cm^{-1} at room temperature, marks the highest values reported for NaSICON separators made via tape casting so far. Furthermore, separators with higher thicknesses nearly double the previously reported values, with a total Na-ion ionic conductivity of 2.44 mS·cm^{-1} at room temperature.

4. Conclusions

For the first time, the additive-free production of undoped NaSICON separators via tape casting with high total Na-ion conductivity was demonstrated. Our free-standing NaSICON separators, with thicknesses from 100 µm to 400 µm, showed outstanding total Na-ion conductivities at room temperature of 1.75 mS·cm^{-1} and 2.44 mS·cm^{-1}, respectively. Nevertheless, a strong influence of the sample thickness on the phase purity as well as on the electrochemical performance was uncovered, caused by the high volatility of Na and P species.

While the self-coating properties of NaSICON during high-temperature treatment were also observed for the tape-cast separators and generally improve the interface resistance between NaSICON and sodium metal, the coating has detrimental effects on the ionic conductivity of the separators when the thickness is reduced to industrially relevant values. Surface modification techniques are thus urgently needed to advance the material towards component production on a large scale and enable industrial Na-ASB cell production.

Supplementary Materials: The following supporting information can be downloaded at: https://www.mdpi.com/article/10.3390/electrochem6010005/s1, Figure S1: Raman measurement of as-prepared surface of tape-cast NaSICON separators and surface after polishing; Table S1: Electrochemical and geometrical data for the equivalent circuit simulation of the impedance measurements.

Author Contributions: Conceptualization: M.R. and M.F.; methodology: M.R.; data curation: S.M., G.D., C.S. and M.R.; formal analysis: S.M., G.D., C.S. and M.R.; funding acquisition: M.F.; project administration: M.F.; resources: M.F.; supervision: M.R. and M.F.; writing—original draft: M.R.; writing—review and editing: M.R., S.M., G.D., C.S. and M.F. All authors have read and agreed to the published version of the manuscript.

Funding: Financial support by the German Federal Ministry of Education and Research (BMBF) within the project MiTemp (13XP0183B) is gratefully acknowledged.

Institutional Review Board Statement: Not applicable.

Informed Consent Statement: Not applicable.

Data Availability Statement: Data is contained within the article or Supplementary Materials.

Acknowledgments: We would like to thank Qianli Ma for performing the temperature-dependent EIS measurements and Yoo Jung Sohn for the grazing incident XRD measurements. We gratefully acknowledge the financial support by the Helmholtz Association and the Federal Ministry of Education and Research (BMBF) within the project MiTemp (Grant No. 13XP0183B).

Conflicts of Interest: The authors declare no conflict of interest.

References

1. European Commission. *European Green Deal—Delivering on Our Target*; Publications Office of the European Union Luxembourg: Luxembourg, 2001.
2. Briant, J.L.; Farrington, G.C. Ionic conductivity in Na^+, K^+, and Ag^+ β″-alumina. *J. Solid State Chem.* **1980**, *33*, 385–390. [CrossRef]
3. Virkar, A.V.; Miller, G.R.; Gordon, R.S. Resistivity-Microstructure Relations in Lithia-Stabilized Polycrystalline β″-Alumina. *J. Am. Ceram. Soc.* **2006**, *61*, 250–252. [CrossRef]
4. Goodenough, J.B.; Hong, H.-P.; Kafalas, J.A. Fast Na^+-ion transport in skeleton structures. *Mater. Res. Bull.* **1976**, *11*, 203–220. [CrossRef]
5. Guin, M.; Tietz, F. Survey of the transport properties of sodium superionic conductor materials for use in sodium batteries. *J. Power Sources* **2015**, *273*, 1056–1064. [CrossRef]
6. Anantharamulu, N.; Rao, K.K.; Rambabu, G.; Kumar, B.V.; Radha, V.; Vithal, M. A wide-ranging review on Nasicon type materials. *J. Mater. Sci.* **2011**, *46*, 2821–2837. [CrossRef]
7. Ma, Q.; Guin, M.; Naqash, S.; Tsai, C.-L.; Tietz, F.; Guillon, O. Scandium-Substituted $Na_3Zr_2(SiO_4)_2(PO_4)$ Prepared by a Solution-Assisted Solid-State Reaction Method as Sodium-Ion Conductors. *Chem. Mater.* **2016**, *28*, 4821–4828. [CrossRef]
8. Ma, Q.; Tsai, C.-L.; Wei, X.-K.; Heggen, M.; Tietz, F.; Irvine, J.T.S. Room temperature demonstration of a sodium superionic conductor with grain conductivity in excess of 0.01 S cm^{-1} and its primary applications in symmetric battery cells. *J. Mater. Chem. A* **2019**, *7*, 7766–7776. [CrossRef]
9. Zhang, Z.; Zou, Z.; Kauo, K.; Xiao, R.; Shi, S.; Avdeev, M.; Hu, Y.S.; Wang, D.; He, B.; Li, H.; et al. Correlated Migration Invokes Higher Na^+-Ion Conductivity in NaSICON-Type Solid Electrolytes. *Adv. Energy Mater.* **2019**, *9*, 1902373. [CrossRef]
10. Ma, Q.; Ortmann, T.; Yang, A.; Sebold, D.; Burkhardt, S.; Rohnke, M.; Tietz, F.; Fattakhova-Rohlfing, D.; Janek, J.; Guillon, O. Enhancing the Dendrite Tolerance of NaSICON Electrolytes by Suppressing Edge Growth of Na Electrode along Ceramic Surface. *Adv. Energy Mater.* **2022**, *12*, 2201680. [CrossRef]
11. Quérel, E.; Seymour, I.D.; Cavallaro, A.; Ma, Q.; Tietz, F.; Aguadero, A. The role of NaSICON surface chemistry in stabilizing fast-charging Na metal solid-state batteries. *J. Phys. Energy* **2021**, *3*, 044007. [CrossRef]
12. Narayanan, S.; Reid, S.; Butler, S.; Thangadurai, V. Sintering temperature, excess sodium, and phosphorous dependencies on morphology and ionic conductivity of NASICON $Na_3Zr_2Si_2PO_{12}$. *Solid State Ion.* **2019**, *331*, 22–29. [CrossRef]
13. Krok, F. Influence of Sintering Conditions on Chemical Composition of Nasicon. *Solid. State Ion.* **1987**, *24*, 21–28. [CrossRef]
14. Gordon, R.S.; Miller, G.R.; McEntire, B.J.; Beck, E.D.; Rasmussen, J.R. Fabrication and characterization of nasicon electrolytes. *Solid. State Ion.* **1981**, *3*, 243–248. [CrossRef]
15. Park, H.; Jung, K.; Nezafati, M.; Kim, C.S.; Kand, B. Sodium Ion Diffusion in Nasicon ($Na_3Zr_2Si_2PO_{12}$) Solid Electrolytes: Effects of Excess Sodium. *ACS Appl. Mater. Interfaces* **2016**, *8*, 27814–27824. [CrossRef] [PubMed]

16. Perthuis, H.; Velasco, G.; Colomban, P. Na^+ and Li^+ NASICON Superionic Conductors Thick Films. *Jpn. J. Appl. Phys.* **1984**, *23*, 534. [CrossRef]
17. Shen, L.; Yang, J.; Liu, G.; Avdeev, M.; Yao, X. High ionic conductivity and dendrite-resistant NASICON solid electrolyte for all-solid-state sodium batteries. *Mater. Today Energy* **2021**, *20*, 100691. [CrossRef]
18. Miyachi, Y.; Sakai, G.; Shimanoe, K.; Yamazoe, N. Fabrication of CO_2 sensor using NASICON thick film. *Sens. Actuators B Chem.* **2003**, *93*, 250–256. [CrossRef]
19. Wang, L. Thick film CO_2 sensors based on Nasicon solid electrolyte. *Solid. State Ion.* **2003**, *158*, 309–315. [CrossRef]
20. Mudenda, S.; Kale, G.M. New insight into the electrical properties and ion dynamics of screen printed NASICON thick films. *J. Mater. Chem. A* **2015**, *3*, 12268–12275. [CrossRef]
21. Ligon, S.C.; Bay, M.C.; Heinz, M.V.F.; Battaglia, C.; Graule, T.; Blugan, G. Large Planar Na-beta″-Al_2O_3 Solid Electrolytes for Next Generation Na-Batteries. *Materials* **2020**, *13*, 433. [CrossRef] [PubMed]
22. Oh, J.A.S.; Xu, X.; Zeng, Z.; Wang, K.; Tan, N.Y.J.; Kok, E.; Huang, J.; Lu, L. Thin NASICON Electrolyte to Realize High Energy Density Solid-State Sodium Metal Battery. *Energy Environ. Mater.* **2023**, *6*, e12472. [CrossRef]
23. Okubo, K.; Wang, H.; Hayashi, K.; Inada, M.; Enomoto, N.; Hasegawa, G.; Osawa, T.; Takamura, H. A dense NASICON sheet prepared by tape-casting and low temperature sintering. *Electrochim. Acta* **2018**, *278*, 176–181. [CrossRef]
24. Naranjo-Balseca, J.M.; Martínez-Cisneros, C.S.; Pandit, B.; Várez, A. High performance NASICON ceramic electrolytes produced by tape-casting and low temperature hot-pressing: Towards sustainable all-solid-state sodium batteries operating at room temperature. *J. Eur. Ceram. Soc.* **2023**, *43*, 4826–4836. [CrossRef]
25. Yang, A.; Ye, R.; Li, X.; Lu, Q.; Song, H.; Grüner, D.; Ma, Q.; Tietz, F.; Fattakhova-Rohlfing, D.; Guillon, O. Fabrication of thin sheets of the sodium superionic conductor $Na_5YSi_4O_{12}$ with tape casting. *Chem. Eng. J.* **2022**, *435*, 134774. [CrossRef]
26. Jaschin, P.W.; Tang, C.R.; Wachsman, E.D. High-rate cycling in 3D dual-doped NASICON architectures toward room-temperature sodium-metal-anode solid-state batteries. *Energy Environ. Sci.* **2024**, *17*, 727–737. [CrossRef]
27. Rosen, M.; Ye, R.; Mann, M.; Lobe, S.; Finsterbusch, M.; Guillon, O.; Fattakhova-Rohlfing, D. Controlling the lithium proton exchange of LLZO to enable reproducible processing and performance optimization. *J. Mater. Chem. A* **2021**, *9*, 4831–4840. [CrossRef]
28. Gross, J.P. Microstructural and mechanical characterization of $Na_{1+x}Hf_2Si_{2.3}P_{0.7}O_{10.85+0.5x}$ and $Na_{1+x}Zr_2P_{3-x}Si_xO_{12}$ NASICON-type solid electrolytes. *J. Mater. Sci.* **2022**, *58*, 144–156. [CrossRef]
29. Loutati, A.; Sohn, Y.J.; Tietz, F. Phase-field Determination of NaSICON Materials in the Quaternary System Na_2O-P_2O_5-SiO_2-ZrO_2: The Series $Na_3Zr_{3-x}Si_2P_xO_{11.5+x/2}$. *Chemphyschem* **2021**, *22*, 995–1007. [CrossRef]